Efficient Method of Moments Analysis of Linear Cavity-Backed Slot Arrays with a Reduced Number of Basis Functions

Geng, Jinglin; Cavallo, Daniele

DOI
10.1109/TAP.2025.3580256

Publication date
2025

Document Version
Final published version

Published in
IEEE Transactions on Antennas and Propagation

Efficient Method-of-Moments Analysis of Linear Cavity-Backed Slot Arrays With a Reduced Number of Basis Functions

Jinglin Geng, *Graduate Student Member, IEEE*, and Daniele Cavallo, *Senior Member, IEEE*

***Abstract*—This work deals with the efficient analysis of linear arrays of cavity-backed slot antennas. The considered array elements can be single or multiple slots radiating in the presence of a rectangular cavity. A spectral method of moments (MoM) is used to estimate the impedance and the patterns of the slot array. The method is rendered computationally efficient by considering, for each slot, only two basis functions that suitably describe the magnetic current distribution. The first basis function is derived by solving the auxiliary problem where only the cavity walls parallel to the slot axes are considered. The second basis function is obtained by solving the problem of a closed rectangular cavity excited by a magnetic current distributed on the slot region. The proposed method allows to simulate entire finite arrays in a few seconds per frequency point and can be exploited to aid the design and optimization of cavity-backed slot arrays.**

***Index Terms*—Cavity-backed slot, method of moments (MoM), slot arrays, spectral-domain method.**

I. Introduction

CAVITY-BACKED slots are common antenna elements in array designs for radar and communication applications. The cavity allows to increase the front-to-back ratio and the gain of the slot elements while isolating the antennas from the surrounding environment. These characteristics are particularly advantageous at millimeter-wave (mmWave) frequencies, for which highly integrated arrays are favorable. The cavity and the metal plane where the slots are etched allow to shield the radiating elements from the electronic circuits, which can be placed closer to the antennas to reduce interconnection losses. Several successful cavity-backed slot array designs have been reported based on various technologies, such as gap waveguide [1], [2], full-metal implementation [3], substrate integrated waveguide [4], printed circuit board [5], and antenna-in-package [6]. These types of arrays can also be scaled to higher frequencies, in the subterahertz range, by exploiting high-precision printed circuit board or advanced packaging technologies [7]. In addition to direct radiating arrays, cavity-backed slots can also be used in combination with quasi-optical systems. For example, in [8], an array of cavity-backed slots is used as a feed array for a dielectric lens antenna.

Concerning the analysis aspects of cavity-backed slots, several approaches have been proposed based on method of moments (MoM) [9], [10], [11], characteristic mode analysis [12], and finite-difference time-domain methods (FDTDs) [13], [14]. However, unlike MoM approaches that discretize only the slots' region, FDTD methods mesh the entire volume, including the space between the slots, with increased complexity for large arrays. One of the advantages of spectral-domain MoM analyses is that they could be combined with stratified media Green's function and easily generalized for slot arrays embedded in dielectric layers.

When specifically considering MoM solutions, however, the works in [9], [10], and [11] considered small-domain basis functions, chosen as piecewise sinusoidal; thus, the computational complexity increases rapidly with the size of the array. Different types of basis functions were considered in other works, e.g., Chebyshev polynomials in [15] or sinusoidal current profiles in [16]. However, these assumptions for the current distribution do not include the reactance at the feed and end points of the slots. The use of two trial functions on the slot, based on a "sin" and "1−cos" profiles, was proposed in [17], but it is not applicable to arbitrary slot length and does not remain valid over large frequency ranges. To describe properly the distribution on the slots with sinusoidal basis functions, the field on the slot was expanded in a series of sinusoids, up to 39 per slot, in [18]. Nevertheless, this approach still results in a large MoM matrix for large arrays.

In this work, we propose a method to greatly reduce the number of basis functions for the analysis of slot arrays with rectangular cavities. We consider only two basis functions per slot element. The two basis functions are resulting from the solution of two auxiliary problems: one is the case where only the cavity walls parallel to the slot axes are considered, while the transverse walls are not present; the second problem assumes the rectangular cavity excited by a magnetic current distributed on the slot region, while the perfectly magnetic conductor is assumed to be above the slot.

The proposed basis functions accurately represent the distribution of the current on the slot over a very large frequency range, even when higher order modes are supported inside the

Received 14 January 2025; revised 27 May 2025; accepted 9 June 2025. Date of publication 23 June 2025; date of current version 14 October 2025. This work was supported by NXP Semiconductors through the Project Sub-THz Antennas for Next Generation Automotive Radars. *(Corresponding author: Jinglin Geng.)*

The authors are with the Microelectronics Department, Faculty of Electrical Engineering, Mathematics and Computer Science, Delft University of Technology, 2628 CD Delft, The Netherlands (e-mail: j.geng@tudelft.nl; d.cavallo@tudelft.nl).

Digital Object Identifier 10.1109/TAP.2025.3580256

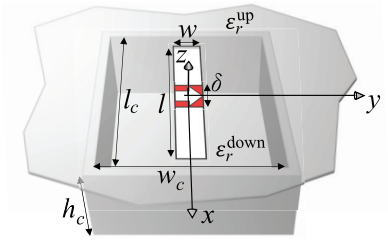

Fig. 1. Cavity-backed slot with defined geometrical parameters.

cavity. The proposed method enables the simulation of entire finite arrays in just a few seconds per frequency point, making it suitable for the design and optimization of cavity-backed slot arrays.

II. Single-Slot Formulation

Let us consider a single slot radiating in the presence of a rectangular cavity with dimensions $w_c \times l_c \times h_c$, as depicted in Fig. 1. The cavity is filled with a dielectric of relative permittivity of $\varepsilon_r^{\text{down}}$. The slot, with length l and width w, is oriented along the x-axis and is excited by a delta-gap generator with length δ. The upper semi-infinite space is assumed to have a relative permittivity of $\varepsilon_r^{\text{up}}$.

From the equivalence theorem, we can replace the original problem with an equivalent problem where the slot region is filled with a perfect electric conductor and a magnetic current density $\vec{m}$ is located above and below the slot region. A magnetic field integral equation can be set up as in [19], by imposing the boundary conditions on the slot plane. For an electrically thin slot, the current is assumed to have only the x-component ($\vec{m} = m_x\hat{x}$). Imposing the boundary conditions for the x-component of the scattered magnetic field on the slot plane results in the following integral equation:

$$\left[m_x * g_{xx}^{\text{up}}\right](x,y) + \left[m_x * g_{xx}^{\text{down}}\right](x,y) = -j_y(x,y) \tag{1}$$

where the scattered magnetic field is expressed as the convolution between the magnetic current and the xx-component of the dyadic space domain Green's functions for the structure above and below the slot (g_{xx}^{up} and g_{xx}^{down}). The term j_y represents the y-component of the surface current density flowing in the feed and the slot terminations. The 2-D convolution can be written explicitly as a double integral over the slots' aperture

$$[m * g](x,y) = \iint_{\text{Slot}} m(x',y')g(x,x',y,y')\mathrm{d}x'\mathrm{d}y'. \tag{2}$$

Observing on the slot axis ($y = 0$), we expand the current in the sum of two basis functions

$$j_y(x,y=0) = i_\delta f_\delta(x) + i_g f_g(x) \tag{3}$$

where f_δ is a function equal to 1 on the delta-gap feed and 0 elsewhere, while f_g is an edge singular distribution describing the diffraction at the slot terminations and its expression can be found in [21]. It should be noted that, in this article, the distribution f_g is assumed to be symmetric at the two ends of the slot, which is only valid if the slot is centered along x with respect to the cavity. However, although not considered here, this assumption can be dropped by considering two independent weights for the two terminations, i.e., $i_g f_g(x)$ becomes $i_{g1}f_{g1}(x) + i_{g2}f_{g2}(x)$.

The coefficient i_δ is assumed to be known, as it represents the amplitude of the impressed current on the feeding gap. Contrarily, the amplitude of the current at the terminations i_g is unknown.

The unknown magnetic current is assumed to be variable separable, i.e.,

$$m_x(x',y') = v(x')m_t(y') \tag{4}$$

where the transverse distribution is assumed to be edge singular $m_t(y') = 2/(w\pi) \times [1-(2y'/w)^2]^{-1/2}$ and the longitudinal distribution $v(x')$ is unknown. By defining the terms

$$d^{\text{up/down}}(x) = \int_{-w/2}^{w/2} m_t(y')g_{xx}^{\text{up/down}}(x,-y')\mathrm{d}y' \tag{5}$$

the integral equation for observing on the slot axis can be written as

$$[d^{\text{up}} * v](x) + [d^{\text{down}} * v](x) = -i_\delta f_\delta(x) - i_g f_g(x) \tag{6}$$

where symbol "*" denotes the 1-D convolution.

Then, we can write the left-hand side and the right-hand side of (6) as inverse Fourier transform (IFT) of their spectral-domain counterpart, following similar steps as [19], [20]:

$$\begin{aligned}&\frac{1}{2\pi}\int_{-\infty}^{\infty} D^{\text{up}}(k_x)V(k_x)e^{-jk_x x}\mathrm{d}k_x \\ &\qquad + \frac{1}{l_c}\sum_{m_x\text{odd}} D^{\text{down}}(k_{xm})V(k_{xm})e^{-jk_{xm}x} \\ &\quad = -\frac{1}{2\pi}\int_{-\infty}^{\infty}[i_\delta F_\delta(k_x) + i_g F_g(k_x)]e^{-jk_x x}\mathrm{d}k_x.\end{aligned} \tag{7}$$

One can note that the spectrum of the scattered field above the slot is continuous and the resulting IFT is an integral. In contrast, the cavity problem leads to a discrete spectrum of the scattered field below the slot so that the corresponding IFT becomes a Floquet sum, where $k_{xm} = -\pi m_x/l_c$ and m_x are odd integers from $-\infty$ to ∞, as described in Appendix A.

The explicit expression of the function D^{up} is known in closed form [19] and is given by

$$D^{\text{up}}(k_x) = \frac{-1}{2k_0\zeta_0}K^2 J_0\left(K\frac{w}{4}\right)H_0^{(2)}\left(K\frac{w}{4}\right) \tag{8}$$

where $K = (k_{\text{up}}^2 - k_x^2)^{1/2}$; $k_{\text{up}} = k_0(\varepsilon_r^{\text{up}})^{1/2}$; k_0 and ζ_0 are the free-space wavenumber and impedance, respectively; J_0 is the zeroth-order Bessel function; and $H_0^{(2)}$ is the Hankel function of zeroth order and the second kind.

The explicit expression of the function D^{down} is derived in Appendix A and is given by a modal expansion, because of the x-oriented cavity walls

$$D^{\text{down}}(k_x) = \frac{k_{\text{down}}^2 - k_x^2}{2w_c k_0\zeta_0}\sum_{m_y=-\infty}^{\infty}\frac{j\cot(k_{zm}h_c)}{k_{zm}}J_0\left(\frac{k_{ym}w}{2}\right) \tag{9}$$

where $k_{\text{down}} = k_0(\varepsilon_r^{\text{down}})^{1/2}$, $k_{ym} = -2\pi m_y/w_c$, and $k_{zm} = (k_{\text{down}}^2 - k_{ym}^2 - k_x^2)^{1/2}$.

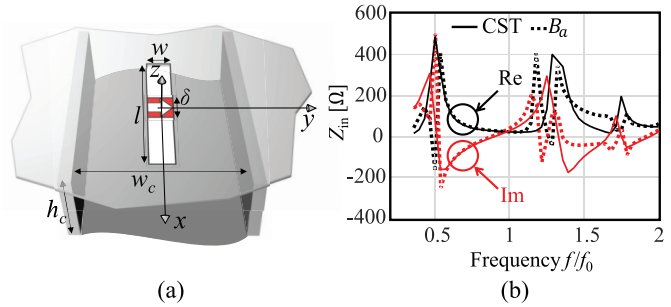

Fig. 2. (a) Auxiliary problem "a" to define the basis function and (b) comparison of the input impedance of the slot between CST and MoM using the basis function B_a.

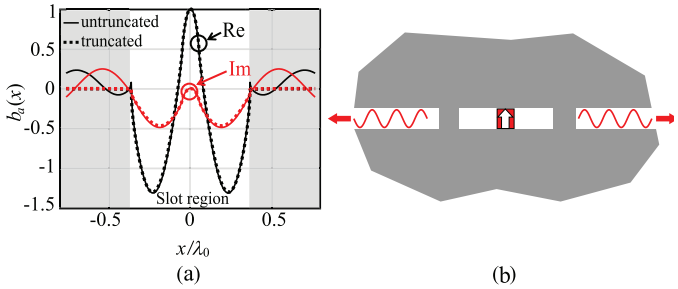

Fig. 3. (a) Solution of the normalized voltage distribution for auxiliary problem "a," with and without truncation, and (b) sketch of the finite metal terminations with unrealistic waves propagating beyond the slot region.

III. Proposed Basis Functions for Single Slot

To solve (7) for the unknown voltage spectrum, one cannot equate the spectra at the left- and right-hand sides as in [22] since the spectrum of the voltage is appearing both in a continuous and a discrete form. To overcome this issue, we propose to expand the unknown voltage in terms of known basis functions that we construct from auxiliary problems.

A. Basis Functions B_a and B_a^{Tr}

As the first attempt, we assume that the voltage spectrum can be expressed as

$$V(k_x) = v_a B_a(k_x) \tag{10}$$

where v_a is an unknown coefficient and the basis function $B_a(k_x)$ is chosen as the normalized solution of an auxiliary problem, which is simpler to solve with respect to the original problem. The auxiliary problem, denoted as "a," is depicted in Fig. 2(a) and represents the same geometry of the original slot, but without the y-oriented walls of the cavities. In this case, the discrete term of (7) becomes continuous, leading to

$$\frac{1}{2\pi}\int_{-\infty}^{\infty}\left(D^{\text{up}}(k_x)+D^{\text{down}}(k_x)\right)V_a(k_x)e^{-jk_x x}\mathrm{d}k_x = -\frac{1}{2\pi}\int_{-\infty}^{\infty}[i_\delta^a F_\delta(k_x)+i_g^a F_g(k_x)]e^{-jk_x x}\mathrm{d}k_x. \tag{11}$$

The voltage spectrum $V_a(k_x)$ for this auxiliary problem can be easily solved by equating the spectra at the left- and right-hand sides of (11) as

$$V_a(k_x) = -\frac{i_\delta^a F_\delta(k_x)+i_g^a F_g(k_x)}{D^{\text{up}}(k_x)+D^{\text{down}}(k_x)}. \tag{12}$$

Weights i_δ^a and i_g^a are not independent, but they should satisfy the condition that the voltage on the slot metal termination is equal to zero. To impose this condition, we defined the projection between two functions $f_1(x)$ and $f_2(x)$ as

$$\langle f_1, f_2\rangle = \int_{-\infty}^{\infty} f_1(x)f_2(x)\mathrm{d}x. \tag{13}$$

It can be shown that the projection can also be evaluated in terms of the Fourier transforms $F_1(k_x)$ and $F_2(k_x)$, as described in [23]

$$\langle f_1, f_2\rangle = \frac{1}{2\pi}\int_{-\infty}^{\infty} F_1(k_x)F_2(-k_x)\mathrm{d}k_x. \tag{14}$$

Thus, projecting the voltage distribution onto the test function f_g associated with the slot terminations and equating to 0 leads to

$$\frac{-1}{2\pi}\int_{-\infty}^{\infty}\frac{i_\delta^a F_\delta(k_x)+i_g^a F_g(k_x)}{D^{\text{up}}(k_x)+D^{\text{down}}(k_x)}F_g(-k_x)\mathrm{d}k_x = 0. \tag{15}$$

From (15), one can find the relation between i_g^a and i_δ^a and express the voltage spectrum as

$$V_a(k_x) = -i_\delta^a\frac{F_\delta(k_x)-\left(Z_{g\delta}^a/Z_{gg}^a\right)F_g(k_x)}{D^{\text{up}}(k_x)+D^{\text{down}}(k_x)} \tag{16}$$

where impedances $Z_{g\delta}^a$ and Z_{gg}^a are defined as

$$Z_{gi}^a = -\frac{1}{2\pi}\int_{-\infty}^{\infty}\frac{F_i(k_x)F_g(-k_x)}{D^{\text{up}}(k_x)+D^{\text{down}}(k_x)}\mathrm{d}k_x \tag{17}$$

with i being either g or δ.

The basis functions $B_a(k_x)$ can be derived by normalizing the voltage spectrum $V_a(k_x)$ such that the IFT of the basis function $b_a(x)$ has an average value of 1 in the feeding gap

$$B_a(k_x) = \frac{V_a(k_x)}{\frac{1}{2\pi}\int_{-\infty}^{\infty}V_a(k_x)F_\delta(-k_x)\mathrm{d}k_x}. \tag{18}$$

One can note that the amplitude of the impressed current on the feeding gap i_δ^a for the auxiliary problem "a" is arbitrary, as it cancels out with the normalization.

By applying Galerkin projection for both sides of (7) onto $B_a(k_x)$ and using (10), one can find the relation between the impressed current and the resulting average voltage across the feeding gap as

$$v_a Y_a = i_\delta^a \tag{19}$$

with

$$Y_a = \frac{1}{2\pi}\int_{-\infty}^{\infty}B_a(-k_x)D^{\text{up}}(k_x)B_a(k_x)\mathrm{d}k_x + \frac{1}{l_c}\sum_{m_x\text{odd}}B_a(-k_{xm})D^{\text{down}}(k_{xm})B_a(k_{xm}) \tag{20}$$

where the input impedance on the feeding gap can simply be found as $Z_{\text{in}} = 1/Y_a$.

Fig. 2(b) shows the comparison of the input impedance computed with commercial software CST and using (20), for a cavity-backed slot with parameters $l = 0.7\lambda_0$, $\delta = 0.1\lambda_0$, $w = 0.06\lambda_0$, $l_c = 0.79\lambda_0$, $w_c = 0.57\lambda_0$, and $h_c = 0.16\lambda_0$, where λ_0 is the wavelength at the frequency f_0 and $\varepsilon_r^{\text{up}} = \varepsilon_r^{\text{down}} = 2.34$.

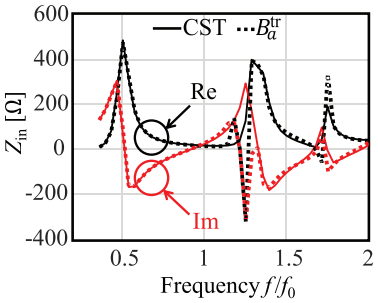

Fig. 4. Comparison of the input impedance of the slot between CST and MoM when using the truncated basis function B_a^{tr}.

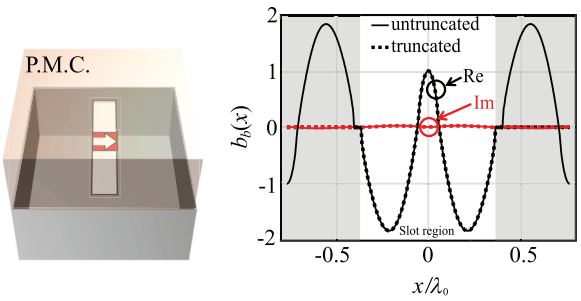

Fig. 5. (a) Auxiliary problem "b" to define the basis functions. (b) Solution of the normalized voltage distribution for auxiliary problem "b" with and without truncation.

It can be seen that the agreement is quite poor. To explain the cause of such inaccuracy, the spatial basis function $b_a(x)$ is plotted in solid lines in Fig. 3(a). One can observe that while the voltage given by the basis function is zero at the slot edges, it continues to exist beyond the slot terminations. This effect is due to the assumption of finite size metal terminations at the slot edges as shown in Fig 3(b). This assumption is convenient because it allows the use of infinite slot spectral Green's function in (8) and (9), as in [21]. However, this results in an unrealistic propagating wave outside the slot region, which contributes to errors in the impedance estimation in the presence of the cavity. Therefore, it is necessary to find the spectrum of the truncated basis function $B_a^{tr}(k_x)$, which includes only the voltage distribution in the slot region. The truncated spectrum can be obtained by convolution with a sinc function as

$$B_a^{tr}(k_x) = \frac{l}{2\pi}\int_{-\infty}^{\infty} B_a\left(k_x'\right)\operatorname{sinc}\left(\frac{\left(k_x - k_x'\right)l}{2}\right)\mathrm{d}k_x'. \tag{21}$$

The evaluation of the integrals in (21) can be computationally expensive, and thus, we resort to an efficient approach to compute $B_a^{tr}(k_x)$ by means of fast Fourier transform (FFT), as described in Appendix B. The resulting truncated voltage distribution is shown in Fig. 3(a) by the dashed curves.

After introducing the truncation of the basis function, the MoM predicts well the input impedance for most of the frequency range, as shown in Fig. 4, except at frequencies around $f = 1.2f_0$ and $f = 1.7f_0$. These discrepancies correspond to higher order resonances being excited in the cavity, which are not accounted for in B_a^{tr} as we consider only the x-oriented wall.

B. Basis Function B_b and B_b^{Tr}

To include the effect of the excited higher order resonances in the cavity, we introduce another basis function B_b^{tr} in the voltage spectrum expansion

$$V(k_x) = v_a B_a^{tr}(k_x) + v_b B_b^{tr}(k_x) \tag{22}$$

where B_b is the solution of a second auxiliary problem "b," in which the original rectangular cavity is located below the slot and a perfect magnetic conductor (PMC) is filling the medium above the slot, as shown in Fig. 5(a). This allows us to isolate only the effect of the x-oriented cavity walls on the slot field distribution. Similar to problem "a," the solution of the voltage spectrum for the second problem $V_b(k_{xm})$ can be found as

$$V_b(k_{xm}) = -i_\delta^b \frac{F_\delta(k_{xm}) - \left(Z_{g\delta}^b / Z_{gg}^b\right) F_g(k_{xm})}{D^{\text{down}}(k_{xm})} \tag{23}$$

with

$$Z_{gi}^b = -\frac{1}{l_c}\sum_{m_x \text{odd}} \frac{F_g(-k_{xm})F_i(k_{xm})}{D^{\text{down}}(k_{xm})} \tag{24}$$

where i can be either g or δ. Then, the untruncated basis function of the second auxiliary problem $B_b(k_{xm})$ can be derived by using a similar normalization as in (18).

It is noted that the untruncated basis function $B_b(k_{xm})$ cannot be used directly in (22) because it is discrete. However, a continuous equivalent of the spectrum can be found by truncating the spatial distribution over the finite slot length. As in (21), this corresponds to a convolution with a sinc function in the spectral domain

$$B_b^{tr}(k_x) = \frac{l}{l_c}\sum_{m_x \text{odd}} B_b(k_{xm})\operatorname{sinc}\left(\frac{(k_x - k_{xm})l}{2}\right). \tag{25}$$

Fig. 5(b) shows the untruncated and truncated solutions of the voltage distribution along the slot for the second auxiliary problem, calculated from $B_b(k_{xm})$ and $B_b^{tr}(k_x)$, respectively. One can note that the untruncated voltage distribution contains periodic replicas with alternatively changing signs, according to the image theorem applied to the y-oriented walls.

Substituting (22) into (7) and projecting with the Galerkin method onto the functions $B_a^{tr}(k_x)$ and $B_b^{tr}(k_x)$, one can solve the unknown v_a and v_b as

$$\begin{bmatrix} v_a \\ v_b \end{bmatrix} = \begin{bmatrix} Y_{aa} & Y_{ab} \\ Y_{ba} & Y_{bb} \end{bmatrix}^{-1} \begin{bmatrix} i_\delta \\ i_\delta \end{bmatrix} \tag{26}$$

with

$$Y_{ij} = Y_{ij}^{\text{up}} + Y_{ij}^{\text{down}} = \frac{1}{2\pi}\int_{-\infty}^{\infty} B_i^{tr}(-k_x)D^{\text{up}}(k_x)B_j^{tr}(k_x)\mathrm{d}k_x + \frac{1}{l_c}\sum_{m_x \text{ odd}} B_i^{tr}(-k_{xm})D^{\text{down}}(k_{xm})B_j^{tr}(k_{xm}) \tag{27}$$

where i and j can be either a or b. The input impedance of the slot can be found as

$$Z_{\text{in}} = \frac{v_a + v_b}{i_\delta}. \tag{28}$$

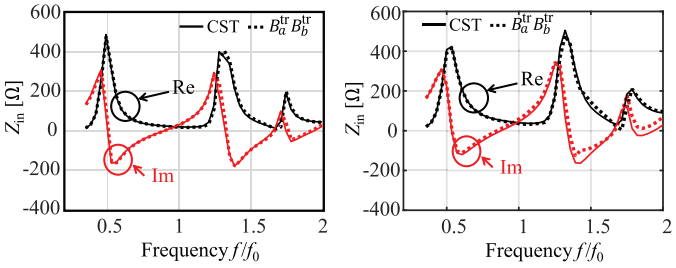

Fig. 6. Comparison of the input impedance of the slot between CST and MoM when using both the truncated basis functions B_a^{tr} and B_b^{tr}. (a) $w = 0.06\lambda_0$. (b) $w = 0.12\lambda_0$.

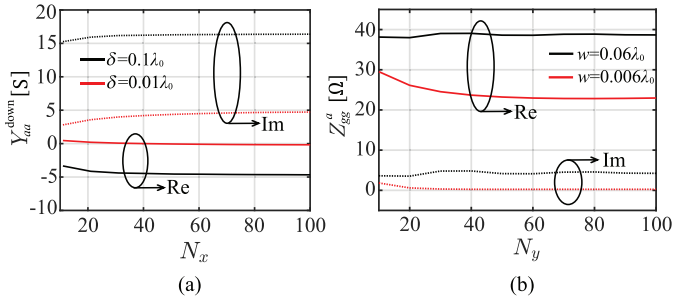

Fig. 7. Convergence of the Floquet sums as a function of modes. (a) Y_{aa}^{down} for slot width $w = 0.06\lambda_0$ and two different feed sizes $\delta = 0.1\lambda_0$ and $\delta = 0.01\lambda_0$. (b) Z_{gg}^{a} for $\delta = 0.1\lambda_0$ and two different values of the slot width $w = 0.06\lambda_0$ and $w = 0.006\lambda_0$.

Fig. 6 shows the input impedance computed by the method in comparison with CST simulations. The parameters in Fig. 6(a) are $l = 0.7\lambda_0$, $\delta = 0.1\lambda_0$, $w = 0.06\lambda_0, l_c = 0.79\lambda_0$, $w_c = 0.57\lambda_0$, and $h_c = 0.16\lambda_0$, where λ_0 is the wavelength at the frequency f_0 and $\varepsilon_r^{up} = \varepsilon_r^{down} = 2.34$. It is seen that the proposed MoM gives an excellent impedance estimation in the entire frequency band, after adding the second type of basis function B_b in the formulation. To highlight the limits of our method, which assumes the slot width to be small with respect to the wavelength, we also consider in Fig. 6(b) the results for a larger slot width $w = 0.12\lambda_0$. The input impedance computed with our method starts to deviate from the CST result at frequencies above $1.4f_0$, for which the width of the slot is around a quarter of the wavelength in the medium.

The solution of the considered problem requires the evaluation of infinite Floquet sums, such as the sum in m_y in (9), used in (17), and the sum in m_x odd to calculate Y_{ij}^{down} in (27). To truncate these sums to a finite number of modes N_x and N_y, we study the convergence of the terms Y_{aa}^{down} and Z_{gg}^{a} in Fig. 7 as a function of N_x and N_y, respectively. It can be seen that the convergence of the sums depends mainly on the electrical size of the feed δ for N_x and on the slot width w for N_y. However, all considered cases require less than 100 modes to converge.

IV. Slot Array

The problem of an array of cavity-backed slots can also be solved with a procedure similar to the single-slot case. In this section, the steps of the single-slot formulation will be generalized to the multiple-slot case. As an example, we consider an array of M double-slot elements radiating in the presence of rectangular cavities, as shown in Fig. 8. The distance between the slots in each double-slot element is indicated by d, while the spacing between the double-slot elements is s.

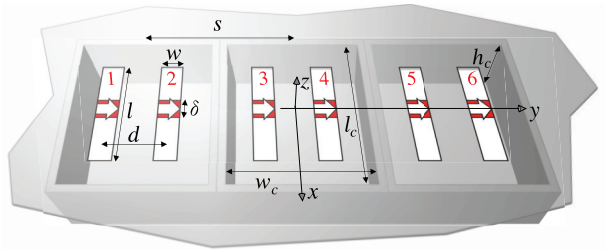

Fig. 8. Array of cavity-backed double slots ($M = 3$) with the definition of the geometrical parameters.

Accounting for the presence of multiple slots, the spectral integral equation in (7), for the mth slot, becomes

$$\sum_{m'=1}^{2M}\left[\frac{1}{2\pi}\int_{-\infty}^{\infty} D_{mm'}^{up}(k_x)V_{m'}(k_x)e^{-jk_x x}\mathrm{d}k_x + \frac{1}{l_c}\sum_{m_x\text{odd}} D_{mm'}^{down}(k_{xm})V_{m'}(k_{xm})e^{-jk_{xm}x}\right] = -\frac{1}{2\pi}\int_{-\infty}^{\infty}[i_{\delta,m}F_\delta(k_x) + i_{g,m}F_g(k_x)]e^{-jk_x x}\mathrm{d}k_x. \quad (29)$$

The explicit expression of the function $D_{mm'}^{up}$ is known in a closed form [22]

$$D_{mm'}^{up}(k_x) = \begin{cases} \dfrac{-1}{2k_0\zeta_0}K^2 J_0\left(K\dfrac{w}{4}\right)H_0^{(2)}\left(K\dfrac{w}{4}\right), & \text{for } m = m' \\ \dfrac{-1}{2k_0\zeta_0}K^2 H_0^{(2)}(K|y_m - y_{m'}|), & \text{for } m \neq m' \end{cases} \quad (30)$$

where y_m and $y_{m'}$ represent the location of the axes of the mth slot and the m'th slot, respectively.

The explicit expression of $D_{mm'}^{down}$ for the double-slot array case is

$$D_{mm'}^{down}(k_x) = \frac{k_{down}^2 - k_x^2}{2w_c k_0\zeta_0}\sum_{m_y=-\infty}^{\infty}\frac{j\cot(k_{zm}h_c)}{k_{zm}}J_0\left(\frac{k_{ym}w}{2}\right) \times\left[1 + e^{-jk_{ym}(w_c-d)}\right]e^{jk_{ym}(y_m - y_{m'})}\alpha_{mm'} \quad (31)$$

where $k_{ym} = -\pi m_y/w_c$, $k_{zm} = (k_{down}^2 - k_{ym}^2 - k_x^2)^{1/2}$, and $\alpha_{mm'} = 1$ if indexes m and m' correspond to slots in the same cavity and 0 otherwise.

A. Formulation

For the sake of compact notation, the integral equations for all slots can be combined in a matrix form as

$$\frac{1}{2\pi}\int_{-\infty}^{\infty}\mathbf{D}^{up}(k_x)\mathbf{V}(k_x)e^{-jk_x x}\mathrm{d}k_x + \frac{1}{l_c}\sum_{m_x\ \text{odd}}\mathbf{D}^{down}(k_{xm})\mathbf{V}(k_{xm})e^{-jk_{xm}x} = -\frac{1}{2\pi}\int_{-\infty}^{\infty}[\mathbf{i}_\delta F_\delta(k_x) + \mathbf{i}_g F_g(k_x)]e^{-jk_x x}\mathrm{d}k_x \quad (32)$$

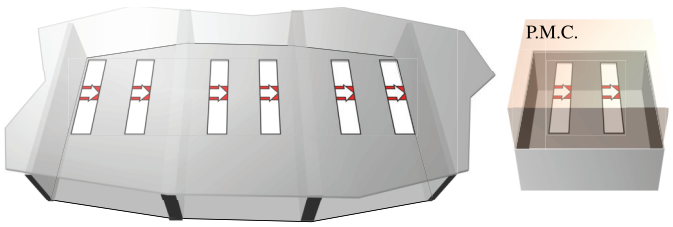

Fig. 9. (a) Sketch of auxiliary problem "a": same slot array without y-oriented walls of the cavity and (b) sketch of auxiliary problem "b": a double-slot element with PMC filling the medium above the slots.

where $\mathbf{D}^{\text{up/down}}$ is the $2M \times 2M$ matrix whose elements are defined in (30) and (31); $\mathbf{V}$ is a column vector with the voltage spectra of each slot, i.e., $\mathbf{V}(k_x) = \{V_1(k_x), V_2(k_x), \ldots, V_{2M}(k_x)\}^T$; and $\mathbf{i}_\delta$ and $\mathbf{i}_g$ are column vectors with currents $i_{\delta,m}$ and $i_{g,m}$, respectively.

Similar to the case of a single slot, we consider the following expansion:

$$\mathbf{V}(k_x) = \mathbf{B}_a^{\text{tr}}(k_x)\mathbf{v}_a + \mathbf{B}_b^{\text{tr}}(k_x)\mathbf{v}_b \tag{33}$$

where matrices $\mathbf{B}_a^{\text{tr}}$ and $\mathbf{B}_b^{\text{tr}}$ are chosen as the solutions of the two auxiliary problems depicted in Fig. 9. The first problem consists of the same slot array, but without the y-oriented walls of the cavities, as shown in Fig. 9(a). For the second problem, we consider that the same cavity is located below the slots and a PMC is filling the medium above the slots, as shown in Fig. 9(b).

Although the steps are not reported for the sake of brevity, a matrix $\mathbf{V}_a$ can be found similar to the case of the single slot as

$$\mathbf{V}_a(k_x) = \left[\mathbf{D}^{\text{up}}(k_x) + \mathbf{D}^{\text{down}}(k_x)\right]^{-1} \times \left[\left(\mathbf{Z}_{gg}^a\right)^{-1}\mathbf{Z}_{g\delta}^a F_g(k_x) - F_\delta(k_x)\mathbf{1}\right] \tag{34}$$

where $\mathbf{1}$ is a matrix of ones of size $2M \times 2M$. This expression results from imposing the condition that the voltage across the slot terminations must be zero and is written in terms of the impedance matrices $\mathbf{Z}_{g\delta}^a$ and $\mathbf{Z}_{gg}^a$, whose elements are defined as

$$Z_{gi,mm'}^a = \frac{-1}{2\pi}\int_{-\infty}^{\infty}\left[\mathbf{D}^{\text{up}}(k_x) + \mathbf{D}^{\text{down}}(k_x)\right]_{mm'}^{-1} \times F_g(-k_x)F_i(k_x)\mathrm{d}k_x \tag{35}$$

where i can be either g or δ. Likewise, the matrix $\mathbf{V}_b$ can be found as

$$\mathbf{V}_b(k_{xm}) = \left[\mathbf{D}^{\text{down}}(k_{xm})\right]^{-1} \times \left[\left(\mathbf{Z}_{gg}^b\right)^{-1}\mathbf{Z}_{g\delta}^b F_g(k_{xm}) - \mathbf{1}F_\delta(k_{xm})\right] \tag{36}$$

with

$$Z_{gi,mm'}^b = -\frac{1}{l_c}\sum_{m_x\ \text{odd}}\left[\mathbf{D}^{\text{down}}(k_{xm})\right]_{mm'}^{-1} F_g(-k_{xm})F_i(k_{xm}) \tag{37}$$

where i can be either g or δ.

The elements of the matrices $\mathbf{V}_a$ and $\mathbf{V}_b$ are modified to impose the truncation of the voltage on the slot region. This is done by applying (66)–(68) for $\mathbf{V}_a$ as described in Appendix B and using (23) for $\mathbf{V}_b$, defining $\mathbf{V}_a^{\text{tr}}(k_x)$ and $\mathbf{V}_b^{\text{tr}}(k_x)$, respectively.

The basis functions are then obtained by normalizing the voltage solutions of the two auxiliary problems as follows:

$$\mathbf{B}_i^{\text{tr}}(k_x) = \left[\frac{1}{2\pi}\int_{-\infty}^{\infty}\mathbf{I}\odot\mathbf{V}_i^{\text{tr}}(k_x)F_\delta(-k_x)\mathrm{d}k_x\right]^{-1}\mathbf{V}_i^{\text{tr}}(k_x) \tag{38}$$

where i is either a or b and $\mathbf{I}$ is the identity matrix of size $2M \times 2M$. Symbol $\odot$ represents the element-wise product between two matrices and the operation $\mathbf{I}\odot\mathbf{V}_i$ maintains only the diagonal elements of the matrix $\mathbf{V}_i$ and gives zeros for the off-diagonal elements.

Substituting (33) into (32) and projecting the mth integral equation onto $B_{a,mm}^{\text{tr}}$ and $B_{b,mm}^{\text{tr}}$, one can solve the unknown $\mathbf{v}_a$ and $\mathbf{v}_b$ as

$$\begin{bmatrix}\mathbf{v}_a\\ \mathbf{v}_b\end{bmatrix} = \begin{bmatrix}\mathbf{Y}_{aa} & \mathbf{Y}_{ab}\\ \mathbf{Y}_{ba} & \mathbf{Y}_{bb}\end{bmatrix}^{-1}\begin{bmatrix}\mathbf{i}_\delta\\ \mathbf{i}_\delta\end{bmatrix} \tag{39}$$

with

$$\mathbf{Y}_{ij} = \frac{1}{2\pi}\int_{-\infty}^{\infty}\left[\mathbf{I}\odot\mathbf{B}_i^{\text{tr}}(-k_x)\right]\mathbf{D}^{\text{up}}(k_x)\mathbf{B}_j^{\text{tr}}(k_x)\mathrm{d}k_x + \frac{1}{l_c}\sum_{m_x\ \text{odd}}\left[\mathbf{I}\odot\mathbf{B}_i^{\text{tr}}(-k_{xm})\right]\mathbf{D}^{\text{down}}(k_{xm})\mathbf{B}_j^{\text{tr}}(k_{xm}) \tag{40}$$

where i and j can be either a or b. Once the unknowns $\mathbf{v}_a$ and $\mathbf{v}_b$ are found, one can obtain the voltage spectrum on each slot from (33) and, by IFT, find the magnetic current density distribution in each slot. Other relevant quantities can be computed, such as mutual coupling, active input impedance, and radiated far field of the array.

1) Mutual Impedance: To find the mutual impedances, we impress the current on the nth slot equal to $i_{\delta,n}$ and zeros elsewhere. By solving the weights of the basis functions using (39) and substituting them in (33), one can obtain the resulting voltage spectra $\mathbf{V}(k_x)$ on each slot due to such current excitation, and then, the average voltage across the mth slot' feeding gap can be found as follows:

$$v_{\delta,m} = \frac{1}{2\pi}\int_{-\infty}^{\infty}V_m(k_x)F_\delta(-k_x)\mathrm{d}k_x. \tag{41}$$

By definition, the term Z_{mn} in the mutual impedance matrix $\mathbf{Z}$ can be obtained as

$$Z_{mn} = \left.\frac{v_{\delta,m}}{i_{\delta,n}}\right|_{i_{\delta,k}=0,\ \text{for}\ k\neq n}. \tag{42}$$

2) Active Input Impedance: Once the impedance matrix $\mathbf{Z}$ is obtained, the active input impedance of each feed can be calculated assuming Norton generators with source currents $i_{\delta,m}$ and impedance Z_L, as shown in Fig. 10. The active current flowing in each of the feeds can be obtained as

$$\mathbf{i}_A = \left[\mathbf{Z} + \mathbf{Z}_L\right]^{-1}\mathbf{Z}_L\mathbf{i}_\delta \tag{43}$$

where $\mathbf{Z}_L$ is a diagonal matrix with its diagonal elements equal to Z_L. Then, the voltage across the feeding gap can be computed as $\mathbf{v}_A = \mathbf{Z}\,\mathbf{i}_A$, and the active impedance at each of the feeding gaps is given by

$$Z_{A,m} = \frac{v_{A,m}}{i_{A,m}}. \tag{44}$$

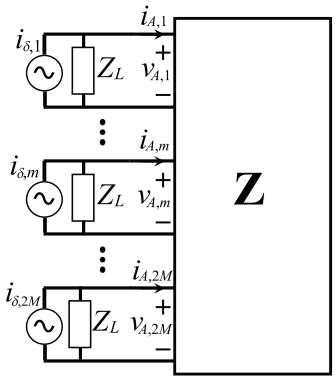

Fig. 10. Norton equivalent circuit of the feeding ports of the array, each connected to a load impedance of Z_L.

TABLE I

COMPARISON OF COMPUTATION TIME AND RELATIVE ERROR BETWEEN CST FREQUENCY-DOMAIN SIMULATIONS AND OUR METHOD

Method	Number of Unknowns	Time	Error
CST	140k	1573 sec	/
CST	114k	1288 sec	4%
CST	103k	1209 sec	11%
CST	65k	877 sec	15%
This work	12	169 sec	8%

3) Radiated Field: Once the active currents flowing in the feeds are known, the voltage spectra $V_{m'}(k_x)$ on each slot can be obtained by using (39) and (33), from which the scattered magnetic field at an arbitrary point (x, y, z) can be calculated using

$$\vec{h}(x,y,z) = \frac{1}{4\pi^2}\int_{-\infty}^{\infty}\int_{-\infty}^{\infty}\bar{\bar{G}}^{\text{up}}(k_x,k_y,z,z')\vec{M}(k_x,k_y) \times e^{-jk_x x}e^{-jk_y y}\mathrm{d}k_x\mathrm{d}k_y \quad (45)$$

where $\bar{\bar{G}}^{\text{up}}$ is magnetic field spectral-domain Green's dyad for a magnetic current on a ground plane; z' is the location of the slot plane; and $\vec{M}(k_x, k_y)$ is the 2-D Fourier transform of the magnetic current, which can be written as

$$\vec{M}(k_x,k_x) = \sum_{m'=1}^{2M} V_{m'}(k_x)M_t(k_y)e^{jk_y y_{m'}}\hat{x} \quad (46)$$

where $M_t(k_y) = J_0(k_y w/2)$.

The radiated far field at an observation point (θ_o, ϕ_o, r_o) can be approximated from (45) using the stationary phase point method as

$$h_\xi(\theta_o,\phi_o,r_o) \approx jk_{zo}G^{\text{up}}_{\xi x}\left(k_{xo},k_{yo},z,z'\right) \times M(k_{xo},k_{yo})e^{jk_{\text{up}}|z-z'|}\frac{e^{-jk_{\text{up}}r_o}}{2\pi r_o} \quad (47)$$

where h_ξ can indicate the x-, y-, or z-component of the radiated magnetic field; $G^{\text{up}}_{\xi x}$ is the ξx component of Green's dyad; $k_{xo} = k_{\text{up}}\sin\theta_o\cos\phi_o$; $k_{yo} = k_{\text{up}}\sin\theta_o\sin\phi_o$; and $k_{zo} = k_{\text{up}}\cos\theta_o$.

B. Validation

To validate the method, an array of three double-slot elements is simulated using CST frequency-domain solver and the proposed method, with each element consisting of two slots backed by a closed cavity, as depicted in Fig. 8. The parameters are $l = 0.7\lambda_0$, $\delta = 0.1\lambda_0$, $w = 0.06\lambda_0$, $l_c = 0.79\lambda_0$, $w_c = 0.57\lambda_0$, $h_c = 0.16\lambda_0$, $\varepsilon_r^{\text{up}} = \varepsilon_r^{\text{down}} = 2.34$, $d = 0.285\lambda_0$, and $s = 0.57\lambda_0$. The two slots of the edge element (indicated as 1 and 2 in Fig. 8) are excited with equal amplitude and phase, while all other slots are passively terminated on a 50-Ω load. Fig. 11 shows a good agreement between our model and CST in terms of active input impedance and the far-field pattern. Table I compares the computation time required to calculate 47 frequency points using CST and our proposed method, for varying mesh settings of CST. Considering the finest mesh (140k cells) as a reference solution, we report the accuracy for different CST simulations with a lower number of mesh cells and our method. The accuracy is defined in terms

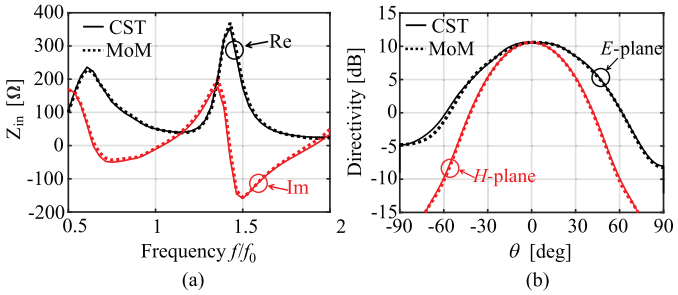

Fig. 11. Comparison between CST and MoM of a three-element cavity-backed double-slot array in terms of (a) active input impedance and (b) directivity of the array at $f = f_0$ when the two slots of the edge element are excited and all other slots are passively terminated.

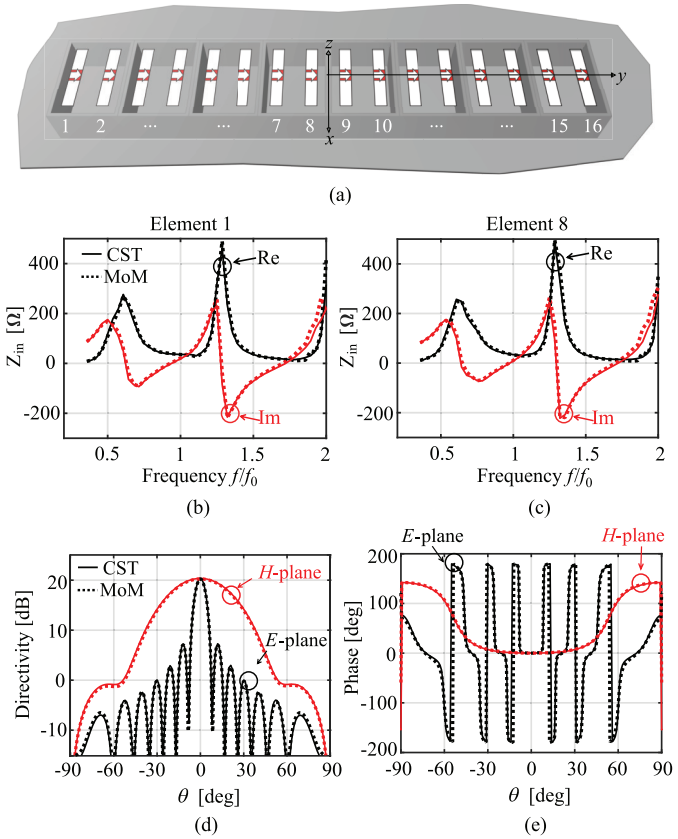

Fig. 12. (a) Array of $M = 8$ cavity-backed double slots. Active input impedance at (b) port 1 and (c) port 8, (d) directivity, and (e) radiated far-field phase of the array at $f = f_0$ when all the elements are excited with equal amplitude and phase.

of the maximum error of active input impedance of the edge slot with respect to the reference CST simulation

$$\epsilon = \frac{\max_f(|Z_{\text{in}} - Z_{\text{ref}}|)}{\max_f(|Z_{\text{ref}}|)}. \tag{48}$$

Our method achieves a speedup factor of 7 with respect to CST, for comparable error. A similar speedup was observed for larger arrays.

Another validation is done for a larger array of eight double-slot elements, as shown in Fig. 12(a), with the same parameters as used in the previous example except for the relative permittivity of the medium filling the cavities, which is now $\varepsilon_r^{\text{down}} = 3.5$. In this case, all 16 slots in the array are excited with the same amplitude and phase. As an example, the computed active input impedances at ports 1 and 8 are plotted in Fig. 12(b) and (c), respectively, as it is seen that they match closely with the results from the CST simulation. The computed radiated far-field properties also exhibit good agreements with the CST finite array simulation, both in terms of directivity and phase patterns, as shown in Fig. 12(d) and (e), demonstrating the accuracy of the method.

V. Conclusion

We presented a numerical method based on spectral-domain MoM for the efficient analysis of linear arrays of cavity-backed slot antennas. To reduce computational complexity, the method employs only two basis functions per slot. The first basis function is determined as the solution of an auxiliary problem considering only the cavity walls parallel to the slot axes, while the second basis function is obtained as the solution of another problem where the slots are located in a closed rectangular cavity.

Validations of the method are done by comparison with CST simulations, demonstrating the method's accuracy in terms of active input impedance and radiation properties. This approach enables the simulation of entire finite arrays within seconds per frequency point, offering significant potential for the design and optimization of such antennas.

Appendix A
Spectral-Domain Representation of Magnetic Field in the Cavity

In this section, we report the steps to derive the spectral-domain expression of the scattered magnetic field in the cavity, used in (7). We start from the expression of the x-component of the scattered magnetic field in the cavity, observed on the slot axis

$$h_x^{\text{down}}(x) = \iint_{\text{Slot}} v(x')m_t(y')g_{xx}^{\text{down}}(x, x', y = 0, y')\mathrm{d}x'\mathrm{d}y'. \tag{49}$$

By applying the image theorem for the vertical walls, we can replace the single current distribution in the cavity with infinite periodic replicas radiating within a parallel plate waveguide, with two infinite ground planes at $z = 0$ and $z = -h_c$

$$h_x^{\text{down}}(x) = \sum_{n_x=-\infty}^{\infty}\sum_{n_y=-\infty}^{\infty}\int_{n_xl_c-l/2}^{n_xl_c+l/2}\int_{n_yw_c-w/2}^{n_yw_c+w/2} v(x')m_t(y') \times g_{xx}^{\text{ppw}}(x - x', -y')\mathrm{d}x'\mathrm{d}y' \tag{50}$$

where g_{xx}^{ppw} is Green's function of the parallel plate waveguide. The periodic current distribution satisfies the following conditions:

$$\begin{aligned} v(x' + n_xl_c) &= (-1)^{n_x}v(x') \\ m_t(y' + n_yw_c) &= m_t(y'). \end{aligned} \tag{51}$$

By using the change of variable $x'' = x' - n_xl_c$ and $y'' = y' - n_yw_c$ and the condition (51), we can write (50) as

$$h_x^{\text{down}}(x) = \sum_{n_x=-\infty}^{\infty}\sum_{n_y=-\infty}^{\infty}\int_{-l/2}^{l/2}\int_{-w/2}^{w/2}(-1)^{n_x}v(x'')m_t(y'') \times g_{xx}^{\text{ppw}}(x - x'' - n_xl_c, -y'' - n_yw_c)\mathrm{d}x''\mathrm{d}y''. \tag{52}$$

Defining d^{down} as

$$d^{\text{down}}(x) = \sum_{n_y=-\infty}^{\infty}\int_{-w/2}^{w/2} m_t(y'')g_{xx}^{\text{ppw}}(x, -y'' - n_yw_c)\mathrm{d}y'' \tag{53}$$

we can write (52) as

$$\begin{aligned} h_x^{\text{down}}(x) &= \left[d^{\text{down}} * v\right](x) \\ &= \sum_{n_x=-\infty}^{\infty}\int_{-l/2}^{l/2}(-1)^{n_x}v(x'')d^{\text{down}} \times (x - x'' - n_xl_c)\mathrm{d}x''. \end{aligned} \tag{54}$$

By introducing the Fourier transforms $D^{\text{down}}(k_x)$ and $V(k_x)$ of $d^{\text{down}}(x)$ and $v(x)$, respectively, we obtain after a few algebraic steps

$$h_x^{\text{down}}(x) = \frac{1}{2\pi}\int_{\infty}^{\infty} D^{\text{down}}(k_x)V(k_x)\sum_{n_x=-\infty}^{\infty}(-1)^{n_x} \times e^{jk_x(n_xl_c-x)}\mathrm{d}k_x \tag{55}$$

where D^{down} can be written as

$$D^{\text{down}}(k_x) = \frac{1}{2\pi}\int_{\infty}^{\infty} G^{\text{ppw}}(k_x, k_y)J_0\left(\frac{k_yw}{2}\right) \times \sum_{n_y=-\infty}^{\infty} e^{jk_yn_yw_c}\mathrm{d}k_y. \tag{56}$$

We now apply the Poisson formula to the infinite sums of exponential terms with indexes n_x and n_y

$$\begin{aligned} \sum_{n_x=-\infty}^{\infty}(-1)^{n_x}e^{jk_xn_xl_c} &= \sum_{n_x=-\infty}^{\infty}e^{jk_x2n_xl_c} - \sum_{n_x=-\infty}^{\infty}e^{jk_x(2n_x-1)l_c} \\ &= (1 - e^{-jk_{xm}l_c})\frac{\pi}{l_c}\sum_{m_x=-\infty}^{\infty}\delta(k_x - k_{xm}) \end{aligned} \tag{57}$$

$$\sum_{n_y=-\infty}^{\infty}e^{jk_yn_yw_c} = \frac{2\pi}{w_c}\sum_{m_y=-\infty}^{\infty}\delta(k_y - k_{ym}) \tag{58}$$

where $k_{ym} = -2\pi m_y/w_c$, $k_{xm} = -\pi m_x/l_c$, and $\delta(k)$ is the Dirac delta function. The term $(1 - e^{-jk_{xm}l_c})$ is equal to 0 when m_x is an even number and is equal to 2 when m_x is an odd number. Therefore, (57) can be written as

$$\sum_{n_x=-\infty}^{\infty}(-1)^{n_x}e^{jk_xn_xl_c} = \frac{2\pi}{l_c}\sum_{m_x\ \text{odd}}\delta(k_x - k_{xm}). \tag{59}$$

Substituting (59) into (55), one can write

$$h_x^{\text{down}}(x) = \frac{1}{l_c} \sum_{m_x \text{ odd}} D^{\text{down}}(k_{xm}) V(k_{xm}) e^{-jk_{xm}x} \tag{60}$$

and by substituting (58) into (56), $D^{\text{down}}(k_x)$ can be written as

$$D^{\text{down}}(k_x) = \frac{1}{w_c} \sum_{m_y=-\infty}^{\infty} G^{\text{ppw}}(k_x, k_{ym}) J_0\left(\frac{k_{ym} w}{2}\right) \tag{61}$$

where the spectral-domain Green's function for the parallel waveguide can be solved using an equivalent transmission line model and results into (9).

Appendix B
Efficient Truncation of the Voltage Solution

As in [22], the truncated spectrum is found by applying an IFT to $V_a(k_x)$, multiplying by a window function with domain $[-l/2, l/2]$, and reapplying a Fourier transform (FT)

$$B_a^{\text{tr}}(k_x) = \int_{-l/2}^{l/2} \left(\frac{1}{2\pi} \int_{-\infty}^{\infty} B_a\left(k_x'\right) e^{-jk_x' x} dk_x' \right) e^{jk_x x} \text{d}x. \tag{62}$$

The double integral in (62) can be expressed as

$$B_a^{\text{tr}}(k_x) = \frac{1}{2\pi} l \int_{-\infty}^{\infty} B_a\left(k_x'\right) \text{sinc}\left(\frac{\left(k_x - k_x'\right) l}{2} \right) \text{d}k_x'. \tag{63}$$

The truncated spectrum in (63) is first computed numerically by discretizing k_x' over the range $(-400k_0, 400k_0)$ using $N_{k_x'} = 10^5$ equidistant points, with a midpoint quadrature rule. This choice of $N_{k_x'}$ resulted from a study on the convergence of the integral. The spectrum values obtained by approximating (63) with the discrete summation, while varying the number of equispaced points in the interval $(-400k_0, 400k_0)$ up to 1.5×10^5, oscillate until convergence is achieved starting at 10^5 points. The spectrum computed with $N_{k_x'} = 10^5$ points is then taken as the reference for accuracy and computation time comparison and is denoted as B_{ref}.

The numerical integral is computationally expensive as it requires a large number of k_x'-integrals, for each value of k_x. However, one can expect that since the truncated and untruncated voltage distributions differ by waves propagating at a significant electrical distance from the feed, the difference between their spectra would asymptotically tend to 0 for large values of k_x. Therefore, one can reduce the number of integrals by only calculating $B_a^{\text{tr}}(k_x)$ for a smaller domain of $k_x \in (-L, L)$, assuming that $B_a^{\text{tr}}(k_x)$ can be approximated as $B_a(k_x)$ for larger values of k_x. Hence, we obtain an approximated solution by imposing

$$B_L(k_x) = \begin{cases} B_{\text{ref}}(k_x), & \text{for } |k_x| \le L \\ B_a(k_x), & \text{for } |k_x| > L. \end{cases} \tag{64}$$

Fig. 13(a) shows the relative error committed by this approximation as a function of the domain of calculation L, where the relative error is ϵ_r defined as

$$\epsilon_r = \sqrt{\frac{\int |B_L(k_x) - B_{\text{ref}}(k_x)|^2 dk_x}{\int |B_{\text{ref}}(k_x)|^2 dk_x}}. \tag{65}$$

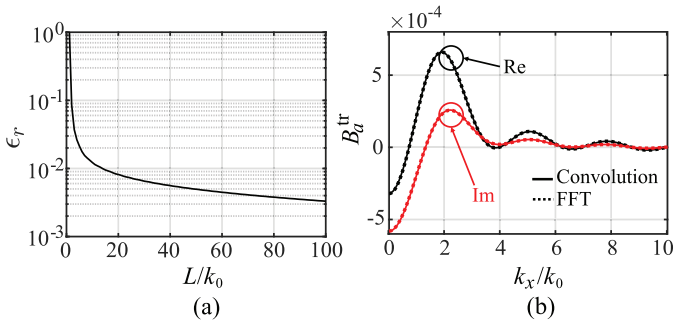

Fig. 13. (a) Real and imaginary parts of the truncated spectrum $B_a^{\text{tr}}(k_x)$. (b) Relative error of compared with $B_a^{\text{tr}}(k_x)$ as a function of calculation domain.

TABLE II
Time and Relative Error Related to the Calculation of the Truncated Spectrum $B_a^{\text{TR}}(k_x)$

Method	Computation Time	Relative Error
No Acceleration	56.5 sec	/
Smaller domain ($L = 40k_0$)	5.5 sec	0.56%
IFFT/FFT	0.003 sec	0.58%

It can be seen that an error $\epsilon_r \approx 0.56\%$ is obtained by choosing $L = 40k_0$, which corresponds to only one tenth of the total number of integrals.

A more efficient method to obtain the truncated spectrum is to replace the IFT and FT operations in (62) with their fast Fourier transform counterparts (FFT and IFFT). First, the spatial-domain voltage distribution is obtained by applying an IFFT on the untruncated spectrum $B_a(k_x)$ in MATLAB

$$b_a(x_n) = \text{ifft}\left\{\text{fftshift}\left\{B_a(k_x)\right\}\right\} \tag{66}$$

where $n = 1, 2, \ldots, N_{k_x}$. The function "fftshift" rearranges the order of elements in $B_a(k_x)$ such that its negative frequency components are mirrored to the right side of the array, which is required by the IFFT process. The resulting spatial sampling x_n also has its negative components mirrored in a similar manner, and it is related to the sampling frequency $k_{x,\text{lim}}$ by $x_n = (n-1)\pi/k_{x,\text{lim}}$. Then, the voltage distribution is truncated by applying a rectangular window that includes only the slot region

$$b_a^{\text{tr}}(x_n) = b_a(x_n) \cdot \text{fftshift}\left\{\text{rect}_l(x_n)\right\} \tag{67}$$

where $\text{rect}_l(x_n)$ is equal to 1 for $x_n \in [-l/2, l/2]$ and 0 otherwise. Finally, the truncated spectrum is obtained by applying an FFT to $b_a^{\text{tr}}(x_n)$ and rearranging its negative frequency components back

$$B_a^{\text{tr}}(k_x) = \text{fftshift}\left\{\text{fft}\left\{b_a^{\text{tr}}(x_n)\right\}\right\}. \tag{68}$$

The resulting truncated spectrum using (68) is plotted in Fig. 13(b), showing an good agreement ($\epsilon_r \approx 0.58\%$) with the reference spectrum $B_{\text{ref}}(k_x)$ that is calculated for the entire domain of k_x using (63).

The computation time and relative error related to the calculation of the truncated spectrum is listed in Table II, showing a clear advantage of the IFFT/FFT method in terms of computation efficiency.

REFERENCES

[1] S. A. Razavi, P.-S. Kildal, L. Xiang, E. A. Alós, and H. Chen, "2×2-slot element for 60 GHz planar array antenna realized on two doubled-sided PCBs using SIW cavity and EBG-type soft surface fed by microstrip-ridge gap waveguide," *IEEE Trans. Antennas Propag.*, vol. 62, no. 9, pp. 4564–4573, Sep. 2014.

[2] J. Liu, A. Vosoogh, A. U. Zaman, and J. Yang, "Design and fabrication of a high-gain 60-GHz cavity-backed slot antenna array fed by inverted microstrip gap waveguide," *IEEE Trans. Antennas Propag.*, vol. 65, no. 4, pp. 2117–2122, Apr. 2017.

[3] R.-S. Chen et al., "High-efficiency and wideband dual-resonance full-metal cavity-backed slot antenna array," *IEEE Antennas Wireless Propag. Lett.*, vol. 19, pp. 1360–1364, 2020.

[4] W. Li, K. D. Xu, X. Tang, Y. Yang, Y. Liu, and Q. H. Liu, "Substrate integrated waveguide cavity-backed slot array antenna using high-order radiation modes for dual-band applications in *K* -Band," *IEEE Trans. Antennas Propag.*, vol. 65, no. 9, pp. 4556–4565, Sep. 2017.

[5] R. M. van Schelven et al., "Phased array with pattern shaping and scan loss reduction for millimeter waves," *IEEE Trans. Antennas Propag.*, vol. 71, no. 1, pp. 159–168, Jan. 2023.

[6] B. Kim, M. Kim, D. Lee, J. Lee, Y. Youn, and W. Hong, "A shared-aperture cavity slot antenna-in-package concept featuring end-fire and broadside radiation for enhanced beam coverage of mmWave mobile devices," *IEEE Trans. Antennas Propag.*, vol. 71, no. 2, pp. 1378–1390, Feb. 2023.

[7] Y. Wang, B. Du, Z. Cao, X. Chen, and H. Meng, "A substrate-integrated cavity-backed slot antenna array in Y-Band," *IEEE Antennas Wireless Propag. Lett.*, vol. 22, pp. 2998–3002, 2023.

[8] J. Geng et al., "Wide scanning lens antenna for sub-terahertz sensing applications," in *Proc. 49th Int. Conf. Infr., Millim., Terahertz Waves (IRMMW-THz)*, Sep. 2024, pp. 1–2.

[9] S. Shi, K. Hirasawa, and Z. Ning Chen, "Circularly polarized rectangularly bent slot antennas backed by a rectangular cavity," *IEEE Trans. Antennas Propag.*, vol. 49, no. 11, pp. 1517–1524, Nov. 2001.

[10] K. W. Leung, "Rectangular and zonal slots on a sphere with a backing shell: Theory and experiment," *IEEE Trans. Antennas Propag.*, vol. 51, no. 7, pp. 1434–1442, Jul. 2003.

[11] H. Morishita, K. Hirasawa, and K. Fujimoto, "Analysis of a cavity-backed annular slot antenna with one point shorted," *IEEE Trans. Antennas Propag.*, vol. 39, no. 10, pp. 1472–1478, Oct. 1991.

[12] C. Guo, Y.-C. Jiao, and Y. Ren, "The substructure characteristic mode analysis for low-profile cavity-backed slot antennas," *IEEE Trans. Antennas Propag.*, vol. 72, no. 8, pp. 6729–6734, Aug. 2024.

[13] T. Hikage, M. Omiya, and K. Itoh, "Considerations on performance evaluation of cavity-backed slot antenna using the FDTD technique," *IEEE Trans. Antennas Propag.*, vol. 49, no. 12, pp. 1712–1717, Dec. 2001.

[14] S. V. Georgakopoulos, C. R. Birtcher, and C. A. Balanis, "Coupling modeling and reduction techniques of cavity-backed slot antennas: FDTD versus measurements," *IEEE Trans. Electromagn. Compat.*, vol. 43, no. 3, pp. 261–272, Aug. 2001.

[15] J. L. Tsalamengas and E. C. Pitsavos, "Diffraction of plane waves by a finite array of dielectric-loaded cavity-backed slots on a common ground plane for oblique incidence and arbitrary polarization," *IEEE Trans. Antennas Propag.*, vol. 52, no. 4, pp. 1070–1079, Apr. 2004.

[16] C. Cockrell, "The input admittance of the rectangular cavity-backed slot antenna," *IEEE Trans. Antennas Propag.*, vol. AP-24, no. 3, pp. 288–294, May 1976.

[17] J. Galejs, "Admittance of a rectangular slot which is backed by a rectangular cavity," *IEEE Trans. Antennas Propag.*, vol. AP-11, no. 2, pp. 119–126, Mar. 1963.

[18] R. Mailloux, "On the use of metallized cavities in printed slot arrays with dielectric substrates," *IEEE Trans. Antennas Propag.*, vol. AP-35, no. 5, pp. 477–487, May 1987.

[19] A. Neto and S. Maci, "Green's function for an infinite slot printed between two homogeneous dielectrics. I. Magnetic currents," *IEEE Trans. Antennas Propag.*, vol. 51, no. 7, pp. 1572–1581, Jul. 2003.

[20] A. Neto and J. J. Lee, "'Infinite bandwidth' long slot array antenna," *IEEE Antennas Wireless Propag. Lett.*, vol. 4, pp. 75–78, 2005.

[21] R. M. van Schelven, D. Cavallo, and A. Neto, "Equivalent circuit models of finite slot antennas," *IEEE Trans. Antennas Propag.*, vol. 67, no. 7, pp. 4367–4376, Jul. 2019.

[22] A. J. van Katwijk, A. Neto, G. Toso, and D. Cavallo, "Efficient semi-analytical method for the analysis of large finite connected slot arrays," *IEEE Trans. Antennas Propag.*, vol. 71, no. 1, pp. 402–410, Jan. 2023.

[23] S. Bruni, N. Llombart, A. Neto, G. Gerini, and S. Maci, "Problem-matched basis functions for microstrip coupled slot arrays based on transmission line Green's functions (TLGF)," *IEEE Trans. Antennas Propag.*, vol. 53, no. 11, pp. 3556–3567, Nov. 2005.

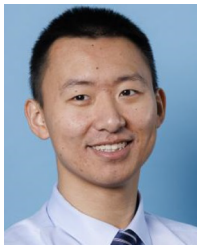

Jinglin Geng (Graduate Student Member, IEEE) received the M.Sc. degree (cum laude) in electrical engineering from Delft University of Technology (TU Delft), Delft, The Netherlands, in 2022, where he is currently pursuing the Ph.D. degree with the Terahertz Sensing Group.

His Ph.D. project focuses on the design of a wide scanning lens antenna for automotive radar applications at 140 GHz. His research interests include method of moments, integrated lens antennas, and robotic antenna measurement systems.

Daniele Cavallo (Senior Member, IEEE) received the M.Sc. degree (summa cum laude) in telecommunication engineering from the University of Sannio, Benevento, Italy, in 2007, and the Ph.D. degree (cum laude) in electromagnetics from Eindhoven University of Technology, Eindhoven, The Netherlands, in 2011.

From 2007 to 2011, he was with the Antenna Group, The Netherlands Organization for Applied Scientific Research, The Hague, The Netherlands. From 2012 to 2015, he was a Post-Doctoral Researcher with the Microelectronics Department, Delft University of Technology (TU Delft), Delft, The Netherlands. In 2015, he joined the Chalmers University of Technology, Gothenburg, Sweden, as a Visiting Researcher. He is currently an Associate Professor with the Terahertz Sensing Group, TU Delft. He has authored or co-authored more than 200 papers published in peer-reviewed international journals and conference proceedings. His current research interests include ultrawideband arrays, electromagnetic modeling of antennas, and millimeter-wave integrated arrays.

Dr. Cavallo received the Best Innovative Paper Prize at European Space Agency Antenna Workshop in 2008, the Best Paper Award in Electromagnetics and Antenna Theory at the 11th European Conference on Antennas and Propagation (EuCAP) in 2017, the Best Antenna Theory Paper at EuCAP 2024, and the "Veni" Personal Grant from the Netherlands Organization for Scientific Research in 2015. His students received the Best Student Paper Award at EuCAP 2013, the Special Mention at EuCAP 2015, the Else Kooi Prize in 2016, the Honorable Mention at the IEEE Antennas and Propagation Symposium in 2019, the Excellent Presentation Award at the IEEE Ukrainian Microwave Conference 2022, and the Van Kinsbergen Prize in 2023. He is the Co-Coordinator of European Association on Antennas and Propagation (EurAAP) working group "Active Array Antennas." He served as the TPC Manager for the International Conference on Infrared, Millimeter and Terahertz Waves in 2022 and the TPC Co-Chair for EuCAP 2024. He has served as an Associate Editor for IEEE TRANSACTIONS ON ANTENNAS AND PROPAGATION from 2016 to 2023.